Modafinil enhances thalamocortical activity by increasing neuronal electrotonic coupling

Francisco J. Urbano*, Elena Leznik†, and Rodolfo R. Llinás‡

Department of Physiology and Neuroscience, New York University Medical Center, 550 First Avenue, New York, NY 10016

Contributed by Rodolfo R. Llinás, June 14, 2007 (sent for review May 10, 2007)

Modafinil (Provigil, Modiodal), an antinarcoleptic and mood-enhancing drug, is shown here to sharpen thalamocortical activity and to increase electrical coupling between cortical interneurons and between nerve cells in the inferior olivary nucleus. After irreversible pharmacological block of connexin permeability (i.e., by using either 18β-glycyrrhetinic derivatives or mefloquine), modafinil restored electrotonic coupling within 30 min. It was further established that this restoration is implemented through a Ca^{2+}/calmodulin protein kinase II-dependent step.

dual-pair recording | *in vitro* | patch clamp | voltage-sensitive dye imaging | Provigil

Modafinil, a (diphenylmethyl) sulfinyl-2 acetamide derivative (also known as Provigil and Modiodal), has recently been used for the treatment of excessive sleepiness associated with narcolepsy (1, 2). Unlike amphetamine, modafinil-induced Fos activation is weak in cortical and thalamic areas as well as in dopamine-responsive areas, such as the striatum (3, 4). Modafinil may also inhibit dopamine 2-like receptors (5) and GABA release (6–10). The latter could be counteracted by serotoneric antagonist pretreatment (6–8, 11). Modafinil action has also been associated with increased glutamatergic, adrenergic, and histaminergic activity (for a review, see ref. 12). Thus, although modafinil has a large potential in neurology and psychiatry, its precise mechanism of action is still unclear.

The thalamocortical system, the most likely target for this drug, is a functionally recurrent neuronal circuit supported by two main interconnected anatomical regions, the thalamus and the cortex. The thalamus is populated by two distinct sets of neurons: cortically projecting relay elements that form glutamatergic excitatory synapses in the cortex which implement a thalamocortical loop, and local thalamic GABAergic neurons (13). The latter, the reticular thalamic neurons and the intrinsic inhibitory interneurons, form two local recurrent inhibitory circuits by recurrent collateral activation from the projecting neurons (14, 15). Corticothalamic afferents activate, very effectively, thalamic relay cell dendrites (16, 17). The recurrent loop is intrinsically oscillatory, both at thalamic as well as cortical levels, and supports inhibitory γ-band rhythmicity. This thalamocortical–corticothalamic system is directly related to functional global brain states (18, 19) in which cellular oscillatory activity is ubiquitous (13, 15). During activated states, noninvasive magnetoencephalographic recordings in humans (20) and *in vivo* recordings in cats (21) indicated that γ-band activity (30–70 Hz) is supported by recurrent activity between thalamic and cortical structures. Aberrations in such thalamocortical dynamics serve as the basis for a wide class of neurological and neuropsychiatric disorders, which have been grouped under the name thalamocortical dysrhythmia syndrome (22).

The neocortex contains pyramidal and nonpyramidal cells that show morphological diversity of dendritic and axonal arborization (23–26). Pyramidal cells are the largest broad class of neurons and provide most of the corticocortical and extracortical projections (26), receiving both excitatory as well as inhibitory postsynaptic potentials (27, 28). The nonpyramidal cells are GABAergic inhibitory interneurons that generate inhibitory postsynaptic potentials (27, 29).

Voltage-sensitive dye imaging (VSDI) experiments demonstrated that inhibitory interneurons play a major role in shaping the cortical activation elicited by afferent inputs (30, 31). Interneurons also exhibit intrinsic oscillatory activity in the γ-band frequency (32), and gap junction block reduces synchrony among them (33). The coexistence of both electrical and chemical synapses between inhibitory interneuron networks allows enhanced timing of spike transmission (34–40). Electrical coupling may contribute to several functional network properties in the cortex, such as spike synchronization and coincidence detection (34, 35, 38, 41–43). However, a too-extensive electrical coupling as initially shown by Connors *et al.* (44) for immature cortex may have a "shunting effect," drastically decreasing the input resistance (45), which explains the absence of epileptiform discharges observed during the first weeks of postnatal development of neocortex (46) when there is extensive electrical coupling.

The aim of this work was to characterize the effects of modafinil on both the thalamocortical and inferior olivary (IO) systems of rodents studied *in vitro* by using VSDI and electrophysiological recordings. Our results indicate that modafinil enhances thalamocortical activity by increasing gap junction coupling between cortical interneurons. A similar effect was observed between IO neurons. Moreover, modafinil-mediated effects required the activation of Ca^{2+}/calmodulin protein kinase II (CaMKII).

Results

Modafinil was applied to cortical (31) or to the more extensive, thalamocortical slices (47) by using either a fast-exchange superperfusion system or local pressure injection onto the tissue. Concentrations ranged between 0.2 and 200 μM, in accordance with previous *in vitro* studies (5, 10, 11). Modafinil effects were observed after 15 min of continuous application and lasted for as long as we continued recording. No significant reversal was observed after $<$30 min of washout.

Cortical and Thalamocortical VSDI. The effects of modafinil were initially studied *in vitro* by using VSDI in coronal slices through the somatosensory cortex, i.e., without thalamic or striatum/putamen synaptic inputs (31). Two bipolar stimulation electrodes were placed on the subcortical white matter to deliver trains of 10-Hz or 40-Hz electrical pulses (Fig. 1*A*). These stimulus frequencies were selected because they had been shown to be optimal in generating wide and columnar cortical activation, respectively (31, 47). VSDI

Author contributions: R.R.L. designed research; F.J.U. and E.L. performed research; F.J.U. and R.R.L. analyzed data; and F.J.U., E.L., and R.R.L. wrote the paper.

The authors declare no conflict of interest.

Freely available online through the PNAS open access option.

Abbreviations: CaMKII, Ca^{2+}/calmodulin protein kinase II; EPSC, excitatory postsynaptic current; IO, inferior olivary; VB, ventrobasal; VSDI, voltage-sensitive dye imaging.

*Present address: Laboratorio de Fisiología y Biología Molecular, Universidad de Buenos Aires-Consejo Nacional de Investigaciones Científicas y Técnicas de Argentina (UBA-CONICET), Buenos Aires, Argentina.

†Present address: Department of Pathology, Taub Institute, Columbia University, New York, NY 10032.

‡To whom correspondence should be addressed. E-mail: llinar01@med.nyu.edu.

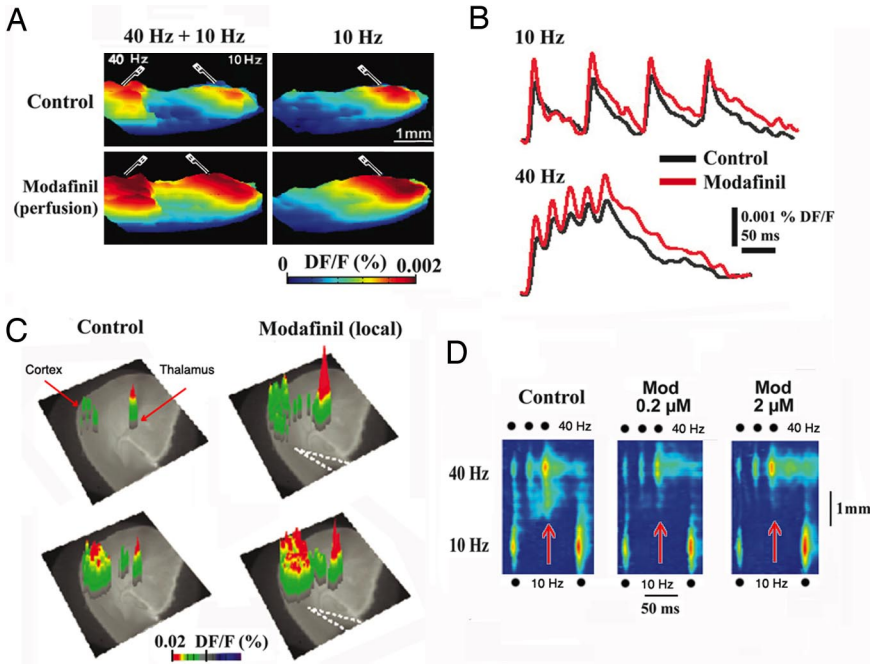

Fig. 1. Modafinil enhances thalamocortical activity and reduces the edge effect *in vitro*. (*A*) Three-dimensional snapshots illustrate voltage-dependent fluorescence image spread, indicating increased cortical activity with paired white matter electrical stimulation at 40 Hz and 10 Hz (*Left*) or with only 10-Hz stimulation (*Right*) before (*Upper*) and after (*Lower*) 100 μM modafinil perfusion. (*B*) Pixel profiles recorded during 10-Hz (*Upper*) and 40-Hz stimulation (*Lower*) before (black) and after modafinil (red) (same slice as in *A*). (*C*) Three-dimensional VSDI elicited by thalamic VB 40-Hz paired shock stimulation before (control; *Left*) and after local micropressure (dotted lines; *Right*) of 100 μM modafinil. The VSDI results are superimposed on a phase-contrast image of the thalamocortical slice. (*D*) Profiles along cortical layer 5 after simultaneous 40-Hz (three pulses) and 10-Hz (two pulses) stimulation in control (*Left*) and 0.2 μM and 2 μM modafinil (*Center* and *Right*). Note the increased response resulting from the interaction of low and high frequencies after the second and third 40-Hz stimuli in the control panel (red arrow). Note how modafinil did reduce such activity (red arrows) (i.e., edge effect) (48).

during the stimulus trains before (Fig. 1*A Upper*) and after (Fig. 1*A Lower*) superfusion of an intermediate concentration of modafinil (100 μM) showed a clear increase in peak amplitude and activated area. The latter increased by 75 ± 9% during the 40-Hz train and by 65 ± 8% during 10-Hz train [$P = 0.009$; $n = 15$ slices (the area was calculated by comparing the size of the cortical region activated, in square millimeters, from 20 to 100% of the maximum activity evoked after the third stimulus of each stimulus train)].

The pixel profile for a small area of cortical layer 5 is shown in Fig. 1*B* before (black) and after (red) modafinil application for each stimulus frequency. The mean increases in the slope of the rising phase of the response to the third shock in the presence of modafinil were 31 ± 4% for stimulation at 10 Hz and 32 ± 3% for stimulation at 40 Hz ($P = 0.03$; $n = 15$ slices).

Local microapplication was found to be an effective drug delivery method (Fig. 1*C*). Thalamic stimulation at 40 Hz elicited a thalamic and cortical VSDI response after the first stimulus (Fig. 1*C Upper Left*) and a larger one after the third stimulus of the train (*Lower Left*). After local modafinil delivery, both the thalamic and cortical responses were increased both after the first thalamic stimulus of the 40-Hz train (Fig. 1*C Upper Right*) and after the third stimulus (*Lower Right*). The VSDI activation profiles along layer 5, displayed as a function of time, are illustrated in Fig. 1*D* during simultaneous 10-Hz and 40-Hz stimulation (electrodes as in Fig. 1*A Left*). These images show facilitated activation of the cortical area between the low- and high-frequency stimulus sites when 10-Hz and 40-Hz stimuli are activated simultaneously. This increased excitability (red arrows) is particularly clear at 40-Hz stimulation (such increased cortical activation is described as an "edge effect" caused by asymmetric lateral inhibition; see refs. 22 and 48). The edge effect was optimally generated with short stimulus pulses (50–75 μs) that, by restricting lateral activation, enhances the interaction area between the 10-Hz and 40-Hz stimulus sites (e.g., Fig. 1*A*). The activation profiles are shown in Fig. 1*D* before and after superfusion with 0.2 μM or 2 μM modafinil. Both concentrations increased the peak amplitude, duration, area, and rate of rise of the activation during stimulation at both frequencies. Modafinil (0.2 μM) increased VSDI signals 70 ± 14% after 10-Hz and 75 ± 11% after 40-Hz stimulation ($P = 0.011$; $n = 7$ slices). Modafinil (0.2 μM) significantly increased the slope of the rising phase of the first response to the 10-Hz stimulation (67 ± 7%; $n = 7$ slices, $P = 0.006$) and 40-Hz stimulation (35 ± 10%; $n = 7$ slices, $P = 0.006$). Indeed, low concentrations were consistently able to facilitate VSDI signals effectively when smaller areas than shown in Fig. 1*A* were activated. Higher concentrations (20–100 μM) of modafinil impaired, rather than facilitated, cortical inhibition (because of excessive electrotonic coupling; see below), producing a clear increment in both the area and slope of the response (data not shown; $n = 5$ slices).

Thalamocortical Interactions in the Absence of Inhibition. Next, we studied the effects of modafinil on excitatory thalamocortical synaptic transmission by blocking inhibitory transmission. Both VSDI and patch clamp whole-cell recordings were implemented in the presence of 100 μM picrotoxin ($GABA_A$ receptor blocker) and 30 μM SCH-50911 ($GABA_B$ receptor blocker). Glutamatergic NMDA receptors were also blocked with 50 μM AP-5 to prevent epileptiform discharges.

By using thalamocortical slices, pixel profiles of VSDI signals were obtained from somatosensory cortex layer 4 after paired stimulation of the ventrobasal (VB) thalamic nucleus delivered at 40 Hz (Fig. 2*A*). A clear facilitation of the cortical fluorescence signal was observed after modafinil application (50–100 μM) as an increase in response amplitude (Fig. 2*A Right*). The time course of the response after the stimuli is shown under control conditions (Fig. 2*B*) and in the presence of modafinil (Fig. 2*C*). AMPA synaptic receptor-mediated excitatory postsynaptic currents (EP-

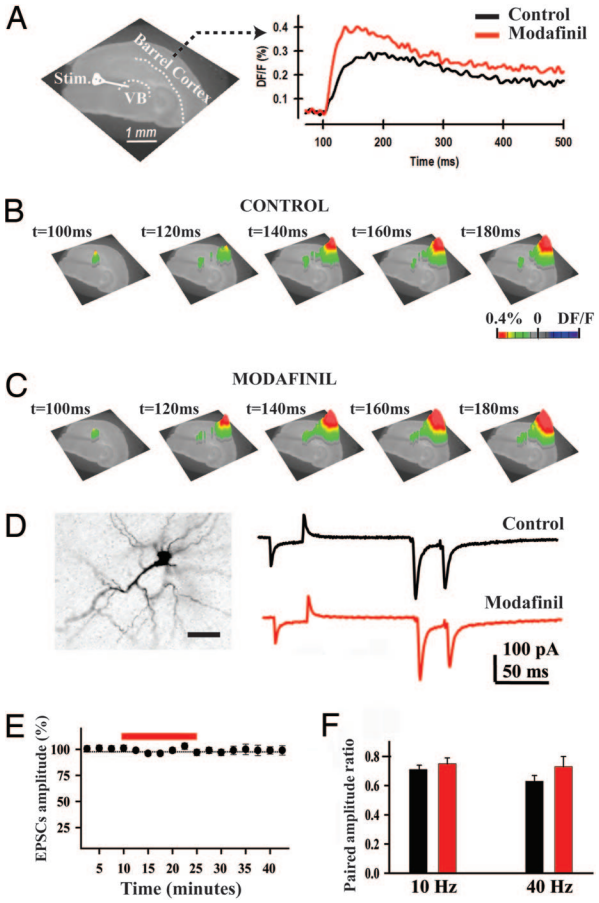

Fig. 2. Modafinil facilitated thalamocortical activity in the absence of GABAergic inhibition. (*A Left*) Phase-contrast image of the thalamocortical slice showing the position of somatosensory barrel cortex and position of the VB stimulation electrode. (*Right*) Fluorescence profiles taken from a layer 4 pixel during paired-pulse stimulation before (black) and after 100 μM modafinil (red) in the presence of $GABA_A$, $GABA_B$, and NMDA blockers. (*B* and *C*) Three-dimensional VSDI images before (Control) and after local micropressure application of 100 μM modafinil (same slice as in *A*). (*D Left*) Representative biocityn-filled layer 4 interneuron. (Scale bar: 50 μm.) (*Right*) Representative EPSC recordings from the same layer 4 neuron before (black) and after a 15-min application of modafinil (red). (*E* and *F*) The EPSC amplitude was not changed over time (*E*), nor did the average amplitude ratios change (*F*).

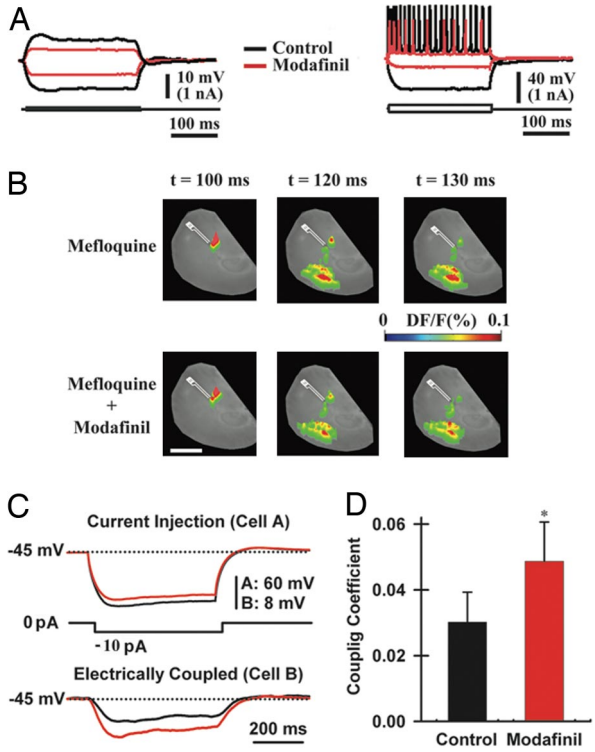

Fig. 3. Modafinil increases electrotonic coupling among cortical interneurons. (*A*) Intracellular recordings from a pyramidal cell (*Left*) and an interneuron (*Right*) before (black) and after 50 μM modafinil (red). (*B*) VSDI responses after 50-min preincubation with mefloquine (50 μM, *Upper*) and 20 min after micropressure application of 50 μM modafinil to the cortex in the presence of mefloquine (*Lower*). (Scale bar, 1 mm.) (*C*) Dual-patch recording from a pair of cortical interneurons (in the presence of 2 μM tetrodotoxin) after the injection of a hyperpolarizing pulse into one neuron (cell A, *Left*) while recording the voltage deflection of the electrically coupled neuron (cell B, *Right*). (*D*) Mean coupling coefficients before (black bar; 0.030 $\pm$ 0.009) and after modafinil application (100 μM, red bar; 0.049 $\pm$ 0.012; $n = 6$ pairs). *, $P = 0.02$.

SCs) were also recorded from layer 4 spiny stellate interneurons before and after application of modafinil by using single-patch recordings. In all VB neurons recorded, a 5-mV hyperpolarizing pulse was systematically applied before synaptic stimulation to determine the stability of whole-cell recordings during the experiment. Strikingly, modafinil significantly increased the input conductance (31 $\pm$ 9%; $n = 15$ neurons) without changing EPSC amplitudes (Fig. 2*D Right*). Modafinil had no affect on EPSCs elicited by paired-pulse VB stimulation at 40 Hz elicited (Fig. 2*E*; same cell as Fig. 2*D*). Average paired amplitude ratios (Fig. 2*F*) did not change during either 10-Hz (control ratio, 0.71 $\pm$ 0.03; modafinil ratio, 0.75 $\pm$ 0.04; $P = 0.1$, $n = 7$ neurons) or 40-Hz stimulation (control ratio, 0.63 $\pm$ 0.04; modafinil ratio, 0.77 $\pm$ 0.07; $P = 0.13$; $n = 8$ neurons).

Electrical Coupling at Cortical Level. Particularly significant was the possibility that modafinil could modulate electrical coupling between cortical neurons. Intracellular recordings were performed in either pyramidal cells or interneurons in the deep cortical layers in rat brain slices. Representative recordings from a pyramidal cell (*Left*) and an interneuron (*Right*) before (Fig. 3*A* black traces) and after (red traces) the application of modafinil show large input conductance changes in both pyramidal cells (*Left*) and interneurons (*Right*) without significant change in the resting potential or time constant. Note that the input resistance of interneurons is higher than that of pyramidal neurons as seen by the large voltage deflection elicited by the hyperpolarizing current pulse (note the difference in the voltage scale in Fig. 3*A*) and the reduction of the number and amplitude of interneuron action potentials (Fig. 3*A Right*). Similar results were observed in 10 cortical pyramidal cells and 3 interneurons.

Given the lack of resting potential or time constant changes that accompanied the input resistance decrease in these cells, the possibility arose that the change could be mediated by changes in electrotonic coupling. This possibility was tested by using the gap junction blockers 18β-glycyrrhetinic acid, its derivative carbenoxolone (100 μM) (49), or mefloquine (25–50 μM) (50). Preincubation of the cortical slices with any of the gap junction blockers did not impair the cortical VSDI fluorescence responses as shown in Fig. 3*B* (*Upper*) for mefloquine (one of seven slices in which this phenomenon was observed). By contrast, mefloquine preincubation reduced the modafinil-induced increment in cortical activation (Fig. 3*B Lower*). Neither 18β-glycyrrhetinic nor carbenoxolone preincubation prevented the effects of modafinil both in VSDI ($n =$ 10 slices) and intracellular recordings ($n = 2$ pyramidal neurons) (data not shown). Furthermore, in seven other slices, the application of either 18β-glycyrrhetinic or carbenoxolone after modafinil

reduced the VSDI responses to control levels. Similar results were obtained by using mefloquine.

Dual Neuronal Impalement of Cortical Interneurons. A wide range of gap junction blockers prevented the effect of modafinil on the thalamocortical system. To investigate directly whether modafinil was augmenting electrotonic coupling, we carried out simultaneous dual whole-cell recording of electrically coupled interneurons in the cortex (Fig. 3*C*). After injection of a hyperpolarizing pulse to one interneuron (Fig. 3*C*, cell A, black trace), the adjacent cell (cell B, black trace) rapidly responded with a smaller change in membrane potential with a similar time course. In the presence of modafinil (Fig. 3*C*, red traces), the voltage in cell A decreased, but that in cell B increased compared with control values (Fig. 3*C*, black traces), indicating increased electrotonic coupling between these cells. Coupling coefficients (51) were calculated as the response amplitude in the coupled cell divided by the amplitude in the injected cell. The mean coupling coefficients were 70% larger in the presence of modafinil (100 μM) (Fig. 3*D*).

Dual Neuronal Impalement of IO Neurons. We studied the effects of modafinil on IO neurons because they are extensively interconnected by dendrodendritic gap junctions (52). IO neurons have been well characterized as generating both synchronous rhythmic firing and coherent subthreshold oscillations (53–57). Modafinil (100–150 μM) reduced the input resistance of IO neurons (Fig. 4*A*, red traces) compared with control conditions (Fig. 4*A*, black traces). Modafinil also brought subthreshold oscillations (Fig. 4*B*, black trace) to suprathreshold for action potential generation (Fig. 4*B*, red trace). The same effects were observed in seven other IO neurons. Note, however, that modafinil did not block the h-current ($n = 4$ neurons). These effects are consistent with an increase in the electrical coupling between IO neurons as seen in interneurons (Fig. 3).

Simultaneous recordings from adjacent IO neurons showed a clear increase in electrotonic coupling (Fig. 4*C Left*, black traces) in the presence of modafinil (Fig. 4*C Left*, red traces). There was a significant difference between the mean coupling coefficients before and after application modafinil (Fig. 4*C Right*).

Molecular Mechanism. To study the molecular mechanism by which modafinil may increase electrotonic coupling, we examined the effect of modafinil in the presence of the gap junction blocker mefloquine. Mefloquine (50 μM; Fig. 4*D*, blue traces) alone increased the input resistance of the injected cell (Fig. 4*D*, cell A, compare black and blue traces) while reducing the amplitude of the voltage step in the coupled cell (Fig. 4*D*, cell B, compare black and blue traces), which indicates that less current was passing between the cells. Application of modafinil after mefloquine further increased the input resistance of cell A while reducing further the input resistance of the coupled cell (Fig. 4*D*, red traces). This effect was seen in three pairs of IO neurons. In one pair of IO neurons, the application of mefloquine after modafinil blocked electrical coupling. These findings indicate that modafinil increases electrical coupling by a mechanism that does not compete with that of mefloquine.

At this point it became important to determine whether modafinil facilitated thalamocortical activity after mefloquine washout. Because mefloquine has been described as slow-acting (50), slices were incubated for 45 min in 20 μM mefloquine and transferred to the recording chamber where they were superfused with artificial cerebrospinal fluid. After 50 min of washout, local application of modafinil increased both the area and intensity of the VSDI signal elicited by 10-Hz white matter stimulation (Fig. 5*A*). This increase was observed in three slices. Larger modafinil-mediated facilitation was seen after a longer period of mefloquine washout in four slices (data not shown). Modafinil not only increased the peak of the response to stimulation but also increased the slope of the response

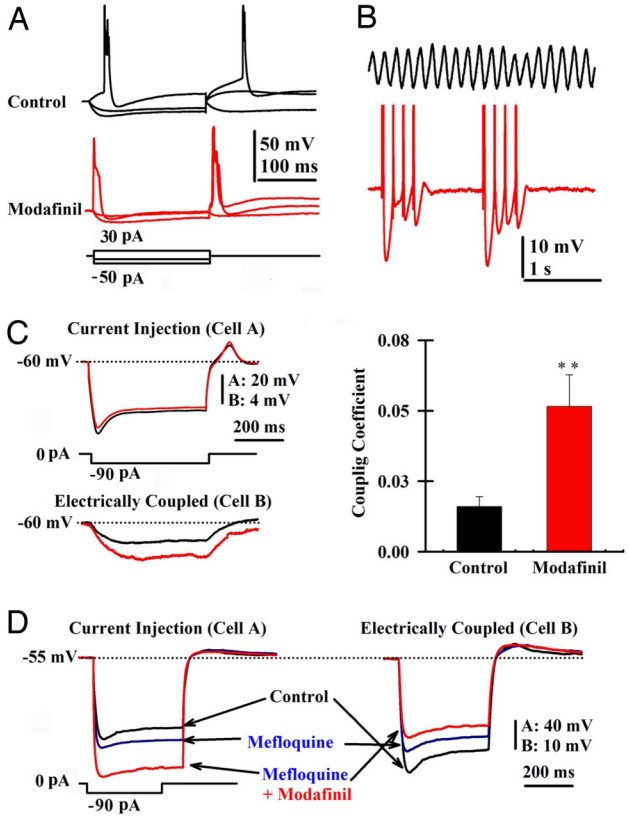

Fig. 4. Modafinil increases electrotonic coupling among IO neurons. (*A*) Single-patch recording of membrane potential changes before (black) and after local modafinil application (150 μM, red). Note the increased input conductance. (*B*) Patch recordings of subthreshold oscillations in an IO neuron in control conditions (7 Hz, black) and after local application of modafinil (red). Modafinil made oscillation amplitude reach action potential threshold. (*C Left*) Superimposed membrane potential responses to a hyperpolarizing pulse before (black) and after modafinil (red) application recorded in a pair of IO neurons. (*Right*) Plot of mean coupling coefficient before (black; 0.016 $\pm$ 0.005) and after modafinil (150 μM, red bar; 0.052 $\pm$ 0.011; $n = 7$ pairs). **, $P = 0.007$. (*D*) Superimposed membrane potential responses in control (black), 50 μM mefloquine, and 150 μM modafinil in the presence of 2 μM tetrodotoxin. Note that the coupled neuron's membrane potential amplitude decreased even in the presence of modafinil.

to the first stimulus from 3.1 DF/F $\times$ ms^{-1} (Fig. 5*B*, black dotted line) to 4.2 DF/F $\times$ ms^{-1} (Fig. 5*B*, red dotted line).

Gap Junction Exteriorization and CaMKII. The ability of modafinil to rescue thalamocortical activity after mefloquine block suggested the possibility that exteriorization of new gap junctions could be the mechanism responsible for the return of electrotonic coupling. Gap junction exteriorization usually requires the activation of intracellular kinase pathways (58–60). In the presence of KN-93 (10 μM, a broad spectrum inhibitor of CaMKII), the VSDI cortical signals were not affected by modafinil, as shown in the VSDI images of the slices (Fig. 5*C*) and pixel profiles (Fig. 5*D*). The same result was observed in six different cortical slices. Modafinil facilitated the VSDI signal in the presence of 2 μM KT5720 (a PKA-selective inhibitor) (data not shown, $n = 3$ slices). Modafinil-dependent increases in the electrotonic coupling between of IO neurons were not seen in the presence of KN-93, although there was a clear depolarizing effect (see membrane potential in Fig. 5*E*), as described recently (61). This effect was seen in two coupled pairs of IO neurons.

In conclusion, modafinil increases electrical coupling by a mechanism that does not compete with mefloquine and depends on a

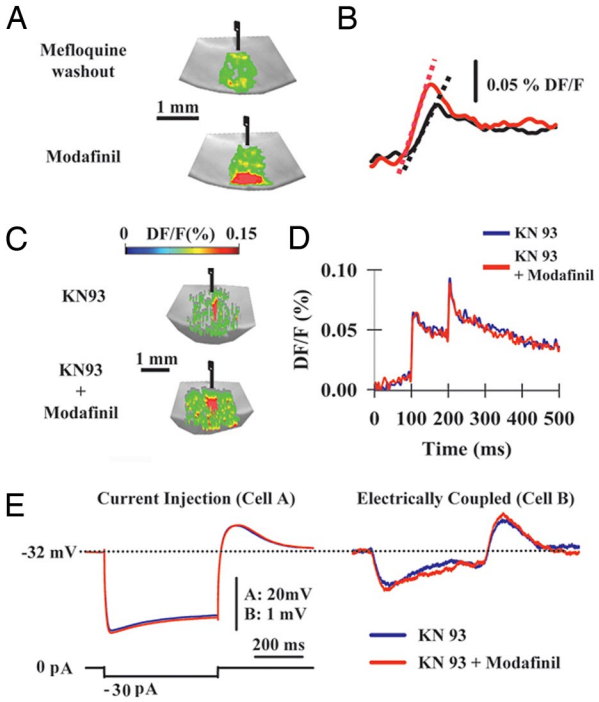

Fig. 5. Modafinil coupling increase is CaMKII-dependent. (*A*) VSDI signals generated by single white matter stimulation after 50-min washout of mefloquine previously incubated at 20 μM for 45 min (*Upper*) and after (*Lower*) the micropressure application of 100 μM modafinil. Modafinil increased both area and amplitude of cortical VSDI responses. (*B*) Pixel profiles after washout of mefloquine and modafinil application shown in *A*. Slopes were 3.1 DF/F $\times$ ms^{-1} and 4.2 DF/F $\times$ ms^{-1} for washout (black line) and modafinil (red line) conditions, respectively. (*C*) VSDI signals generated in the presence of 10 μM KN-93 (inhibitor of CaMKII) and KN-93 + modafinil. (*D*) Pixel profiles in the presence of KN-93 (blue line) and KN-93 + modafinil (red line). (*E*) Superimposed responses of a dual-patch recorded pair of IO neurons (in 2 μM tetrodotoxin) in the presence of KN-93 (blue lines) and KN-93 + modafinil (red lines). The low resting potential is because of the presence of KN-93 (61).

CaMKII, most probably involving the exteriorization of new gap junction hemichannels.

Discussion

The pharmacological mechanism by which modafinil acts as both an antinarcoleptic and mood-enhancing drug is still under scrutiny. Modafinil has been proposed to act on the GABAergic inhibitory network of the thamalocortical system, in agreement with the previously described effect on GABAergic networks in sleep and non-sleep-related areas (6–10).

The data presented here offer several lines of evidence for a mechanism of action for modafinil that results in increased electrotonic coupling, as demonstrated in cortical interneurons and in IO neurons. The effect of this drug, administered by superfusion or micropressure injection, is consistent with a time-dependent waxing of the direct electrical current flow between neurons in the CNS. The effects of this increased coupling can be demonstrated both by means of voltage-dependent dye imaging and paired simultaneous recordings of coupled neurons. Although our results could suggest possible direct effects on membrane permeability, given the sizable change in input conductance for both interneurons and pyramidal cells, no change in resting potential or membrane time constant was observed. Concerning the unexpected results indicating increased pyramidal cell coupling given that only the "same type" of GABAergic neurons is anticipated to be electrically coupled at cortical levels (35–38, 41–43), the findings may be an age-related issue. Indeed, the intracellular recordings presented here were performed in cortical slices from juvenile animals postnatal days 10–18 (51), which may explain the presence of functional gap junctions in pyramidal neurons (44, 45). Moreover, direct coupling has been shown among pyramidal neurons in slices from older rats (62) and electrical coupling among excitatory neurons and inhibitory neurons in somatosensory cortex (e.g., ref. 40). Additionally, modafinil may be mediating a *de novo* exteriorization of gap junction proteins in pyramidal neurons. In this sense, the fact that modafinil increased the electrical coupling by a mechanism that does not compete with mefloquine and that this effect depends on a CaMKII supports such hypothesis. Indeed, as demonstrated by previous investigators, up-regulation of connexin43 in spinal cord astrocytes (58) and of connexin35 (a fish ortholog of the mammalian connexin36) in goldfish Mauthner cells (60) was CaMKII activation-dependent, although a variety of kinases can also reduce the coupling between AII Amacrine cells in mouse retina, which is mediated by connexin36 (59).

Although modafinil improves wakefulness in patients suffering from narcolepsy, shift work sleep deprivation, and other sleep disorders (12), its effectiveness may be related to the fact that subcoeruleus neurons, which are involved in the transitions between sleep and wake states, are electrically coupled (63). The finding is also consistent with the fact that cortical interneurons are extensively coupled (36–38, 41–43), so the drug may help in the generation of the lateral inhibition that seems to be associated with γ-band activity and its relation to cognition (48)

From a motor point of view, the presence of continuous subthreshold oscillations in IO neurons has also been found to require electrical coupling (64–66). Given the role of oscillations in cerebellar motor function (64), a modafinil-dependent increment in electrotonic coupling may mediate the observed improvement in motor tasks in patients receiving this agent (67).

Finally, the effects of modafinil on the thalamocortical system described here are consistent with the previously described cognitive enhancement by this drug in healthy adults (68) and with the positive effects in patients with thalamocortical dysrhythmia syndrome (69, 70). Indeed, we described here how modafinil can reduce the edge effect in cortical slices, a phenomenon proposed to be the basis for the abnormal wave coherence between low (δ- and θ-band) and high frequencies (β- and γ-bands) in patients presenting with thalamocortical dysrhythmia syndrome (22, 48).

Materials and Methods

Preparation of Slices. Animal use and experimental methods were approved by the Institutional Animal Care and Use Committee of the New York University School of Medicine. All animals were anesthetized with pentobarbital (120 mg/kg i.p.) and decapitated after loss of the limb-withdrawal reflex. Thalamocortical slices (350–400 μM) were obtained from black C57BL/6 mice (either sex, P7–20; Taconic Farms, Germantown, NY) (47). Cortical slices (300–450 μm) were collected from the somatosensory "barrel" cortex of Sprague–Dawley rats (either sex, P10–18; Taconic Farms) (31). Parasagittal brainstem slices containing the IO were prepared from Long–Evans rats (P6–14) following protocols from previous *in vitro* studies (52, 65). Slices were allowed to recover at 35°C for at least 30 min. The chamber contained a continuously oxygenated normal artificial cerebrospinal fluid (124 mM NaCl/5 mM KCl/1.25 mM KH_2PO4/26 mM $NaHCO_3$/1.2 mM $MgCl_2$/ 2.4 mM $CaCl_2$/10 mM glucose, pH 7.4). Experiments were conducted at a bath temperature of 32°C.

Intracellular Recordings. Intracellular recordings were obtained by using glass micropipettes filled with 3 M potassium acetate. Electrodes were advanced by using a Narashige manipulator, and signals were amplified with an Axoclamp-2A amplifier (Molecular Devices, Sunnyvale, CA) and acquired at 10 kHz with a digital oscilloscope (Nicolet 4094; Nicolet Instrument Co., Madison, WI) for off-line computer analysis. Intracellular data were analyzed

by using IGOR Pro-based software (WaveMetrics, Inc., Lake Oswego, OR).

Recording and Analysis of VSDI Signals. VSDI recording were obtained as described previously (31, 47). Slices were stained with either the voltage-sensitive dye RH 414 or di-4ANEPPS (0.025 mg/ml; Molecular Probes, Eugene, OR). Optical signals were monitored with either fast CCD camera HR Deltaron 1700, Fujix (MathWorks, Inc., Natick, MA) or MICAM Ultima (1 ms per frame, vs. 0703, BrainVision, Inc, Irvine, CA). Changes in membrane potentials were evaluated as fractional fluorescence, DF/F ($F - F_o/F$, where F_o is the base fluorescence level). Movies were analyzed off-line, and the viewpoint of the signals was changed from the default value of 90° to 45° to display VSDI signals as 3D figures.

Patch Recordings. Coupling was studied in cortical interneurons and IO neurons by injecting negative current pulses into one neuron of a pair and recording the voltage response in both neurons of the pair. Because voltage deflection of coupled neurons ranged from <1 mV to a few mV, the mean of 10–20 individual trials is displayed. Coupling coefficients were calculated as the response amplitude in the noninjected cell divided by the response amplitude in the injected cell. Patch recordings were made at 32°C in a fast-exchange chamber (3–4 ml/min). Neuron pairs were chosen by eye based on the proximity of their somata. Patch electrodes were made from borosilicate glass and had resistances of 3–10 MΩ when filled with a high potassium intracellular solution (130 mM $KMeSO_3$/10 mM NaCl/10 mM Hepes/1 mM EGTA/4 mM MgATP/0.4 mM NaGTP/2 mM $MgCl_2$/10 mM sucrose/10 mM phosphocreatine, pH 7.3, 290 mOsm). Amino-3-hydroxy-5-methyl-4-isoxazolepropionic acid-mediated synaptic currents were recorded with a high cesium/QX314 (high Cs^+) intracellular solution (120 mM $CsMeSO_3$/8 mM NaCl/10 mM Hepes/5 mM EGTA/10 mM tetraethylammonium chloride/4 mM MgATP/0.5 mM GTP/7 mM phosphocreatine, pH 7.3, 290 mOsm). Recordings were achieved by using a motorized multimicromanipulator MPC200/ROE200 (Sutter Instrument, Novato, CA) attached to a MultiClamp 700B amplifier (Molecular Devices) in combination with the PCLAMP 10.0 software (Molecular Devices). Biocytin was sometimes included in the intracellular solution to permit characterization of the recorded neuron's morphology by using the ABC kit-DAB method.

Pharmacological Reagents. Drugs were purchased from Sigma–Aldrich (St. Louis, MO). KT5720 was purchased from EMD Biosciences (La Jolla, CA). KN-93 was purchased from Tocris (Ellisville, MO). The voltage-sensitive dyes were purchased from Molecular Probes. Mefloquine was provided by the Drug Synthesis and Chemistry Branch, Developmental Therapeutics Program, National Cancer Institute, National Institutes of Health (Bethesda, MD).

Statistical Analysis. Sigmaplot 10.0 (Systat Software, Inc., San Jose, CA) was used for statistical analysis. Statistics were performed with two-tailed unpaired and paired Student's t tests. Differences were considered significant if at least $P < 0.05$. Population statistics are presented here as mean ± SEM.

We thank Dr. Robert J. Schultz (Drug Synthesis and Chemistry Branch, National Cancer Institute, National Institutes of Health, Bethesda, MD) for supplying mefloquine. This work was supported by National Institutes of Health Grant NS13742 (to R.R.L.).

1. US Modafinil Multicenter Study Group (1998) *Ann Neurol* 43:88–97.
2. US Modafinil Multicenter Study Group (2000) *Neurology* 54:1166–1175.
3. Lin J-S, Hou Y, Jouvet M (1996) *Proc Natl Acad Sci USA* 93:14128–14133.
4. Scammell TE, Estabrooke IV, McCarthy MT, Chemelli RM, Yanagisawa M, Miller MS, Saper CB (2000) *J Neurosci* 20:8620–8628.
5. Korotkova TM, Klyuch BP, Ponomarenko AA, Lin JS, Haas HL, Sergeeva OA (2007) *Neuropharmacology* 52:626–633.
6. Tanganelli S, Fuxe K, Ferraro L, Janson AM, Bianchi C (1992) *Naunyn-Schmiedeberg's Arch Pharmacol* 345:461–465.
7. Tanganelli S, Perez de la Mora M, Ferraro L, Mendez-Franco J, Beani L, Rambert FA, Fuxe K (1995) *Eur J Pharmacol* 273:63–71.
8. Ferraro L, Tanganelli S, O'Connor WT, Antonelli T, Rambert F, Fuxe K (1996) *Neurosci Lett* 220:5–8.
9. Ferraro L, Antonelli T, O'Connor WT, Tanganelli S, Rambert FA, Fuxe K (1998) *Neurosci Lett* 253:135–138.
10. Ferraro L, Antonelli T, Tanganelli S, O'Connor WT, Perez de la Mora M, Mendez-Franco J, Rambert FA, Fuxe K (1999) *Neuropsychopharmacology* 20:347–356.
11. Ferraro L, Fuxe K, Tanganelli S, Fernandez M, Rambert FA, Antonelli T (2000) *Neuropharmacology* 39:1974–1983.
12. Ballon JS, Feifel D (2006) *J Clin Psychiatry* 67:554–566.
13. Jones EG (2007) *The Thalamus* (Cambridge Univ Press, Cambridge, UK), 2nd Ed.
14. Steriade M, Parent A, Hada J (1984) *Comp Neurol* 229:531–547.
15. Steriade M (2000) *Neuroscience* 101:243–276.
16. Pedroarena CM, Llinás RR (1997) *Proc Natl Acad Sci USA* 94:724–728.
17. Pedroarena CM, Llinás RR (2001) *Thalamus Relat Syst* 1:3–14.
18. Llinás R, Pare D (1991) *Neuroscience* 44:521–535.
19. Llinás RR, Ribary U, Contreras D, Pedroarena C (1998) *Philos Trans R Soc London B* 353:1841–1849.
20. Ribary U, Ioannides AA, Singh KD, Hasson R, Bolton JP, Lado F, Mogilner A, Llinás RR (1991) *Proc Natl Acad Sci USA* 88:11037–11041.
21. Steriade M, Amzica F (1996) *Proc Natl Acad Sci USA* 93:2533–2538.
22. Llinás R, Ribary U, Jeanmonod D, Kronberg E, Mitra PP (1999) *Proc Natl Acad Sci USA* 96:15222–15227.
23. Ramón y Cajal S (1911) *Histology of the Nervous System* (Oxford Univ Press, New York), Vol 2.
24. Jones EG (1975) *J Comp Neurol* 160:205–268.
25. DeFelipe J (1993) *Cereb Cortex* 3:273–289.
26. DeFelipe J, Fariñas I (1992) *Prog Neurobiol* 39:563–607.
27. Connors BW, Malenka RC, Silva LR (1988) *J Physiol (London)* 406:443–468.
28. McCormick DA (1989) *J Neurophysiol* 62:1018–1027.
29. McCormick DA, Connors BW, Lighthall JW, Prince DA (1985) *J Neurophysiol* 54:782–806.
30. Laaris N, Carlson GC, Keller A (2000) *J Neurosci* 20:1529–1537.
31. Contreras D, Llinás R (2001) *J Neurosci* 21:9403–9413.
32. Llinás RR, Grace AA, Yarom Y (1991) *Proc Natl Acad Sci USA* 88:897–901.
33. Traub RD, Kopell N, Bibbig A, Buhl EH, LeBeau FEN, Whittington MA (2001) *J Neurosci* 21:9478–9486.
34. Bartos M, Vida I, Frotscher M, Geiger JR, Jonas P (2001) *J Neurosci* 21:2687–2698.
35. Gallarreta M, Hestrin S (1999) *Nature* 402:72–75.
36. Gallarreta M, Hestrin S (2001) *Science* 292:2295–2299.
37. Gallarreta M, Hestrin S (2001) *Nat Rev Neurosci* 2:425–433.
38. Gibson JR, Beierlein M, Connors BW (1999) *Nature* 402:75–79.
39. Tamas G, Buhl EH, Lorincz A, Somogyi P (2000) *Nat Neurosci* 3:366–371.
40. Venance L, Rozov A, Blatow M, Burnashev N, Feldmeyer D, Monyer H (2000) *Proc Natl Acad Sci USA* 97:10260–10265.
41. Fricker D, Miles R (2001) *Neuron* 32:771–774.
42. Spruston N (2001) *Neuron* 31: 669–671.
43. Rouach N, Avignone E, Meme W, Koulakoff A, Venance L, Blomstrand F, Giaume C (2002) *Biol Cell* 94:457–475.
44. Connors BW, Benardo LS, Prince DA (1983) *J Neurosci* 3:773–782.
45. Peinado A, Yuste R, Katz LC (1993) *Neuron* 10:103–114.
46. Sutor B, Hablitz JJ, Rucker F, tenBruggencate G (1994) *J Neurophysiol* 72:1756–1768.
47. Llinás RR, Leznik E, Urbano FJ (2002) *Proc Natl Acad Sci USA* 99:449–454.
48. Llinás RR, Urbano FJ, Leznik E, Ramirez RR, van Marle HJF (2005) *Trends Neurosci* 28:325–333.
49. Davidson JS, Baumgarten IM (1988) *J Pharmacol Exp Ther* 246:1104–1107.
50. Cruikshank SJ, Hopperstad M, Younger M, Connors BW, Spray DC, Srinivas M (2004) *Proc Natl Acad Sci USA* 101:12364–12369.
51. Bennett MV, Zukin RS (2004) *Neuron* 41:495–511.
52. Sotelo C, Llinás R, Baker R (1974) *J Neurophysiol* 37:541–559.
53. Llinás R, Yarom Y (1981) *J Physiol (London)* 315:549–567.
54. Llinás R, Yarom Y (1986) *J Physiol (London)* 376:163–182.
55. Benardo LS, Foster RE (1986) *Brain Res Bull* 17:773–784.
56. Llinás R, Sasaki K (1989) *Eur J Neurosci* 1:587–602.
57. Leznik E, Makarenko V, Llinás R (2002) *J Neurosci* 22:2804–2815.
58. De Pina-Benabou MA, Srinivas M, Spray DC, Scemes E (2001) *J Neurosci* 21:6635–6643.
59. Urschel S, Höher T, Schubert T, Alev C, Söhl G, Wörsdörfer P, Asahara T, Dermietzel R, Weiler R, Willecke K (2006) *J Biol Chem* 281:33163–33171.
60. Pereda AE, Bell TD, Chang BH, Czernik AJ, Nairn AC, Soderling TR, Faber DS (1998) *Proc Natl Acad Sci USA* 95:13272–13277.
61. Rezazadeh S, Claydon TW, Fedida D (2006) *J Pharmacol Exp Ther* 317:292–299.
62. MacVicar BA, Dudek FE (1981) *Science* 213:782–785.
63. Heister DS, Hayar A, Charlesworth A, Yates C, Zhou YH, Garcia-Rill E (2007) *J Neurophysiol* 97:3142–3147.
64. Blenkinsop TA, Lang EJ (2006) *J Neurosci* 26:1739–1748.
65. Leznik E, Llinás RR (2005) *J Neurophysiol* 94:2447–2456.
66. Placantonakis DG, Bukovsky AA, Aicher SA, Kiem H-P, Welsh JP (2006) *J Neurosci* 26:5008–5016.
67. Llinás R, Welsh JP (1993) *Curr Opin Neurobiol* 3:958–965.
68. Turner DC, Robbins TW, Clark L, Aron AR, Dowson J, Sahakian BJ (2003) *Psychopharmacology* 165:260–269.
69. Nieves AV, Lang A (2002) *Clin Neuropharmacol* 25:111–114.
70. Rosenthal MH, Bryant SL (2004) *Clin Neuropharmacol* 27:38–43.